ARTICLE

Green light activated dual-action Pt(IV) prodrug with enhanced PDT activity

Received 00th January 20xx,
Accepted 00th January 20xx

DOI: 10.1039/x0xx00000x

Daniil Spector,[a] Vladislav Bykusov,[a] Yulia Isaeva,[b,c] Roman Akasov,[b,c] Anastasia Zharova,[a] Igor Rodin,[a] Mikhail Vokuev,[a] Vita Nikitina,[a] Alexander Martynov,[d] Elena Beloglazkina,[a] Olga Krasnovskaya [a*]

Light induced release of cisplatin from Pt(IV) prodrugs is a promising tool for precise spatiotemporal control over the antiproliferative activity of Pt-based chemotherapeutic drugs. A combination of light-controlled chemotherapy (PACT) and photodynamic therapy (PDT) in one molecule has the potential to overcome crucial drawbacks of both Pt-based chemotherapy and PDT via synergetic effect. Herein we report green-light activated Pt(IV) prodrugs **GreenPt** with BODIPY-based photosentitizer in axial position with incredible high light response and singlet oxygen generation ability. **GreenPt** demonstrated the ability to release cisplatin under low-dose green light irradiation up to 1 J/cm^2. The investigation of the photoreduction mechanism of **GreenPt** prodrug using DFT modeling and ΔG_0 PET estimation revealed that the anion-radical formation and substituent photoinduced electron transfer from the triplet excited state of the BODIPY axial ligand to the Pt(IV) center is the key step in the light-induced release of cisplatin. Green-light activated BODIPY-based photosentitizers **5** and **8** demonstrated outstanding photosensitizing properties with extraordinary phototoxicity index (PI) >1300. **GreenPt** prodrug demonstrated gradual intracellular accumulation and light-induced phototoxicity with PI > 100, thus demonstrating dual action through light-controlled release of both cisplatin and a potent BODIPY-based photosensitizer.

Keywords: Prodrug, photoactivation, cisplatin, BODIPY, PDT

Introduction

In the last few decades, a great progress in anticancer therapy was achieved thanks to the widespread use of DNA-alkylating Pt(II) drugs, such as cisplatin (CDDP) and its analogues, carboplatin and oxaliplatin.[1–3] Despite high efficacy and broad applicability of platinum(II)-based agents, those drugs possess crucial drawbacks such as low selectivity and poor bloodstream stability, which results in adverse side effects.[4–6] In addition, prolonged Pt(II)-based chemotherapy leads to acquired resistance of tumors, thus limiting their application in clinic.[7,8] Therefore, the development of next-generation platinum-based antitumor agents with improved antitumor efficiency is of great importance.

Pt(IV) complexes are considered as the next-generation platinum antitumor drugs, capable of overcoming drug resistance.[9–11] Kinetic stability of the octahedral Pt(IV) complexes results in enhanced intracellular penetration, while high variability of axial ligands opens path to multi-action antitumor agents with enhanced biological activity.[12,13] On the other hand, Pt (IV) complexes are also possessing low selectivity and prone to rapid reduction in the bloodstream; as a result their therapeutic effectiveness is almost indistinguishable from that of the parent Pt(II) complex.[14,15] Thus, uncontrolled and premature release of the cytotoxic Pt(II) complex from Pt(IV) prodrug leads to pronounced toxicity of Pt(IV) prodrugs and complicates their clinical use.

A light-induced activation of Pt(IV) prodrugs is an elegant approach that allows spatial and temporal control over the release of Pt(II) drug. In this drug design, photoabsorbers are used as axial ligands of Pt(IV) prodrugs; resulted Pt(IV) prodrugs are stable and non-toxic in the dark, and release cytotoxic Pt(II) drug only under light irradiation, thus acting as agents of PACT.[16,17] To date, a number of Pt(IV) prodrugs with different photoabsorbers in the axial position have been reported. Among the photoabsorbers used, BODIPY attracts attention due to their unique photophysical properties, such as high fluorescence quantum yields and exceptional optical and thermal stability. Importantly, a unique feature of BODIPY is the ability to fine-tune their photophysical properties through easy and straightforward post-functional modifications.[18,19] In particular, the introduction of a heavy atom increases the probability of the spin-forbidden transition $S_1 \rightarrow T_1$ and intersystem crossing (the "heavy atom effect").[20–22] As a result, halogenated BODIPY capable of triplet state stabilization are widely used in the design of photosentitizers (PS).[23] Upon irradiation of nontoxic photosensitizers in a certain area, the production of cytotoxic reactive oxygen species (ROS) take place; this phenomenon is the basis of Type II PDT.[24,25]

The undoubted advantage of PDT is its external controllability, i.e. the ability to localize its action in space and time. However, its dependence on the presence of oxygen to provide a therapeutic effect limits the therapeutic effect of PDT. In order to overcome this limitation, a combination of PDT and chemotherapy/PACT could be proposed. Thus, one PDT/PACT agent could possess light-controlled synergistic action. For this

[a] Chemistry Department, Lomonosov Moscow State University, Leninskie gory 1,3, 119991 Moscow, Russia;
[b] I.M. Sechenov First Moscow State Medical University, Trubetskaya 8-2, Moscow, 119991, Russia;
[c] Moscow Pedagogical State University, 119435, Malaya Pirogovskaya str. 1, Moscow, Russia;
[d] Frumkin Institute of Physical Chemistry and Electrochemistry, Russian Academy of Sciences, Leninskii pr., 31, bldg. 4, 119071, Moscow, Russia.
† Footnotes relating to the title and/or authors should appear here.
Supplementary Information available. See DOI: 10.1039/x0xx00000x

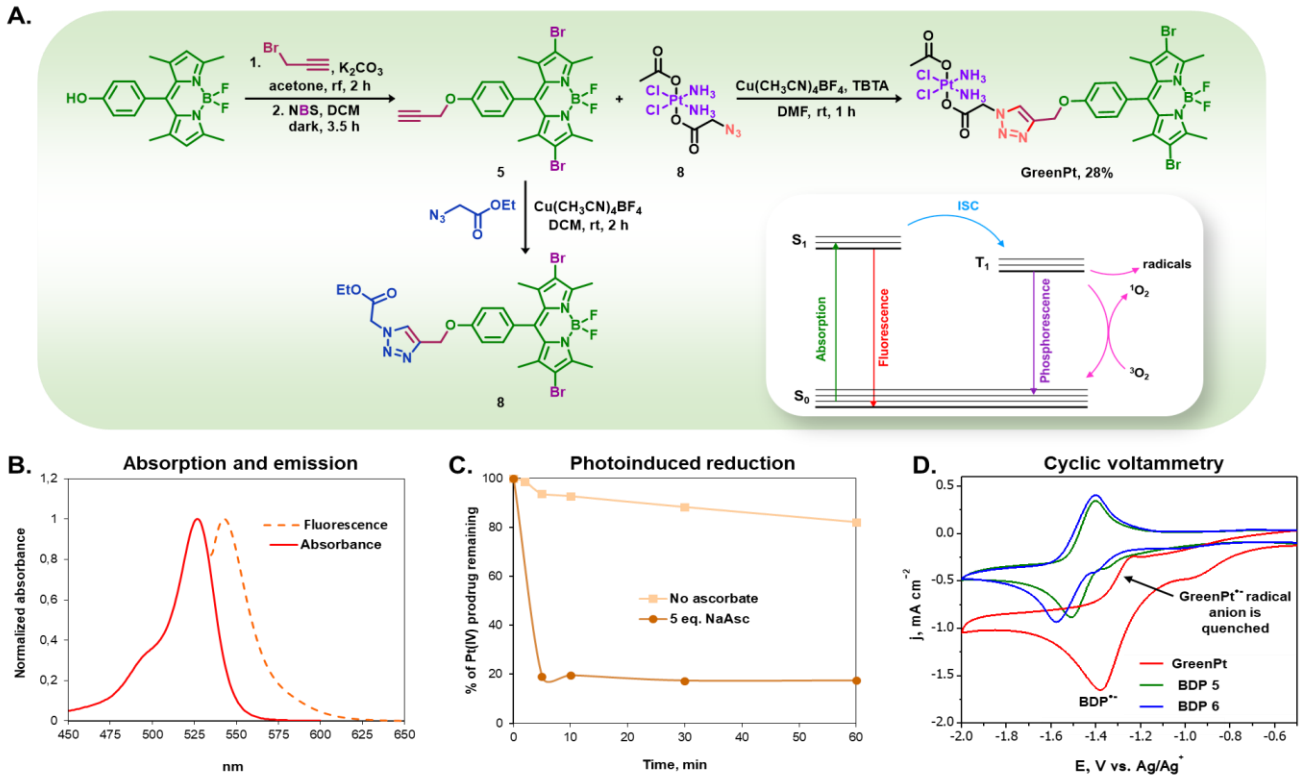

Figure 1. A. **GreenPt** synthesis scheme. **B**. Absorption and emission spectra of **GreenPt** in DMSO (2 mM). **C**. **GreenPt** decay under green light irradiation (530 nm, 6.5 mW/cm^2) in the absence and in the presence of sodium ascorbate (1 mM in 75:25:5 DMSO:MeOH:H_2O). **D**. CVA curves of **GreenPt** and BODIPYs **5** and **6** in DCM (2 mM) with Bu_4NBF_4 (0.1 M) on a glassy carbon electrode.

purpose, PS capable of light-induced ROS generation could be used as an axial ligand for Pt(IV) prodrugs, thereby yielding Pt(IV) prodrugs with dual photodynamic/photochemotherapeutic action.[26,27] In recent years, several photoactivable Pt(IV) prodrugs with BODIPYs as an axial ligand were designed.[28–32] Nevertheless, the double action Pt(IV) prodrugs with the ROS-producing BODIPY moiety in axial position have not yet been reported.

Herein, we designed a novel green light activated dual-action Pt(IV) prodrug **GreenPt** with PDT-active BODIPY as an axial ligand. Under green light irradiation, **GreenPt** releases cisplatin; on the other hand, **GreenPt** prodrug is an effective photosensitizer with high phototoxicity index (PI), that demonstrates toxicity in the nanomolar range and high quantum yield of singlet oxygen. This is the first example of dual axial Pt(IV) prodrug with PACT/PDT activity with BODIPY-based photosensitiser in axial position.

Results and discussion

Design and synthesis. To conjugate a PDT-active BODIPY with the Pt(IV) center the Cu-catalyzed click-reaction was used, which was also utilized recently to obtain blue-light activated Pt(IV) prodrugs.[30] Thus, BODIPY **5** with terminal alkyne group and heavy bromine atoms at the 2,6 positions of the BODIPY core was synthesized following slightly modified literature procedures.[33] **GreenPt** was obtained via click reaction between BODIPY **5** and Pt(IV) complex **7** with azide group in the axial position. Triazole-bearing BODIPY **8** was also obtained via click reaction of BODIPY **5** with methyl 2-azidoacetate (SI, Schemes S1, S2). The structures of all compounds obtained were confirmed by ^{1}H, ^{13}C NMR and HRMS (SI, Figures S1-S19). Purity of **GreenPt** (>95%) was confirmed via HPLC (SI, Figures S20-S21).

Photophysical properties and TDDFT calculations. Photophysical properties of **GreenPt** complex and BODIPY **8** were studied; both compounds showed similar absorption and fluorescence spectra with absorption maximum at 527 nm and emission at 543 nm (Table 1, Figure 1B, SI, Figure S22). Fluorescence quantum yields were 0.17 and 0.25 for **GreenPt** and **5**, respectively. A decrease in fluorescence quantum yield value of **GreenPt** when compared to BODIPY **5** could indicate either the photoinduced electron transfer from singlet excited state of ^{1}BODIPY* ligand to the Pt(IV) center, or efficient intersystem crossing from S_1 to T_1 state in **GreenPt**. In 2020, Zhu et al. reported a similar green-light activated Pt(IV) complex "BODI-Pt", based on carboplatin with a non-brominated BODIPY moiety in axial position. However, the emission of BODI-Pt was totally quenched, thus suggesting a direct electron transfer from a singlet excited state ^{1}BODIPY* to the Pt(IV) center. [28] TDDFT calculations performed for **GreenPt** and BODIPY **5** argues against the possibility of intramolecular charge transfer (ICT),

Table 1. Photophysical properties of BODIPY **8** and **GreenPt**

Compound	λ_{abs}, max nm[a]	Molar absorption coefficient ε (M^{-1}*cm^{-1})	λ_{fl}, max, nm[a]	Stokes Shift	Fluorescence quantum yield F_{fl}[b]	Singlet oxygen quantum yield Φ_D[c]
BODIPY 8	527	95400	543	16	0.25	0.69
GreenPt	527	73200	543	16	0.17	0.63

[a] Measured in DMSO

[b] Measured in toluene

[c] Measured in acetonitrile

since the wavefunctions corresponding to the excitations of both molecules are almost 100% pure excitation from HOMO to LUMO. In turn, these frontier orbitals are localized exclusively on the chromophoric part of the molecule and the Pt(IV)-localized orbitals are located above the LUMO on the energetic scale (Figure 2).

Triplet-triplet absorption and Singlet oxygen generation. Triplet-triplet absorption spectra for both **GreenPt** and BODIPY **5** were obtained via flash-photolysis, and showed long-lived triplet states with lifetimes 416 ns and 390 ns, respectively, which are close to the previously reported values (Figures S23-S24, SI).[34] Since **GreenPt** and BODIPY **5** were designed as heavy atom photosensitizers, capable of spin–orbit coupling (SOC) triplet excited state T_1 formation, they are expected to generate singlet oxygen upon light irradiation. Thus, singlet oxygen quantum yields for **GreenPt** and BODIPY **5** were determined via singlet oxygen phosphorescence, and were found to be 0.63 and 0.69, respectively (Table 1, Figure S25, SI). Thus, both compounds are expected to act as highly potent triplet photosensitizers and generate cytotoxic ROS under green light irradiation. Also, TDDFT calculations confirmed that both BODIPY **5** and **GreenPt** retain the SOC values typical for other reported halogenated BODIPY derivatives[35] – 0.81 and 0.84 cm^{-1} respectively, while their S_1 and T_1 excited levels have equivalent energies – 2.66 and 1.41 eV respectively for both compounds. Other triplet states have higher energies compared to S_1 state and they do not contribute to photodynamic action.

GreenPt stability studies. Pt(IV) octahedral prodrugs exhibit cytotoxic effect upon intracellular reduction and release of DNA-alkylating agent cisplatin as well as axial ligands. Thus, susceptibility of Pt(IV) prodrugs towards hydrolysis and reduction is a key property that affects the overall antitumor profile of the complex.[14,36] Pt(IV) prodrugs with photoactive ligands should be stable in the dark, while rapidly releasing cisplatin under visible light irradiation.[16,37] Thus, we first evaluated the stability of **GreenPt** in the dark in the absence, as well as in the presence of sodium ascorbate, a common biological reducing agent with elevated concentrations in cancer cells.[38,39] When no sodium ascorbate was present in the solution, **GreenPt** complex showed no decay for 24 hours, indicating its great stability towards hydrolysis. In the presence of 5 equivalents of sodium ascorbate, a slow reduction of the complex was observed, and 70% of Pt(IV) prodrug remained in the solution after 24 hours (Figure S26, A). As expected, the accumulation of cisplatin in the solution was observed as the prodrug was reduced, which was detected via LCMS as cisplatin with one of the chloride ligands exchanged for DMSO (m/z 342.0010 (Figure S26, B, S27, SI). It is worth noting that **GreenPt** is quite resistant to reduction since axial carboxylate groups do not form bridges with the reducing agent, which facilitate hydride transfer.[40]

Photoactivation properties of GreenPt. Light-induced reduction of Pt(IV) prodrugs depends greatly on the nature of the photoactive axial ligand. After excitation, the ligand could act as a reducing agent, donating an electron at the Pt(IV) center and turning into the radical cation.[30,41] When that is the case, the photoreduction rate of the prodrug is independent of the presence of an electron-donor. Another photoreduction path

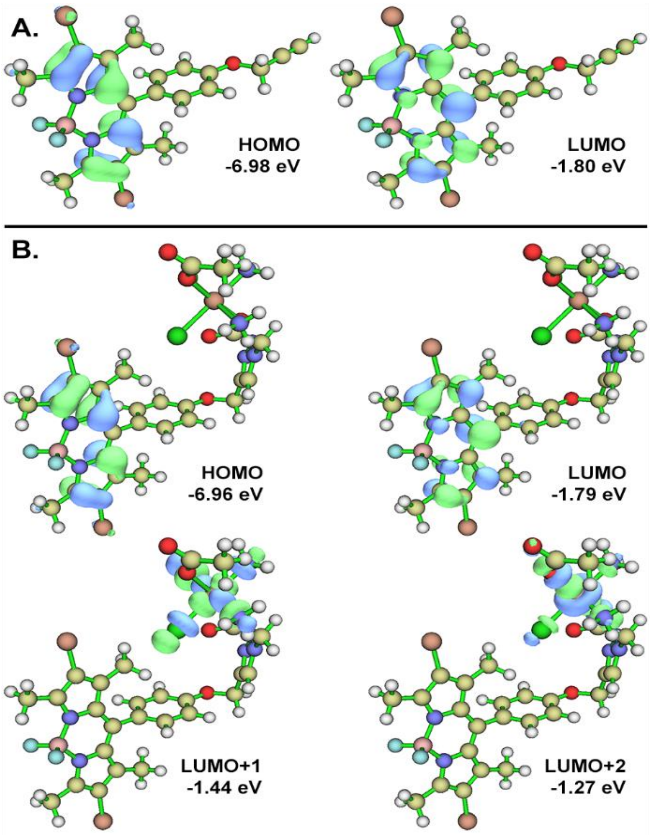

Figure 2. Frontier orbitals of BODIPY **5** – **A** and **GreenPt** – **B** calculated at CAM-B3LPY/ZORA-def2-TZVP for light elements and SARC-ZORA-TZVP for Pt level of theory.

requires an intermolecular reaction between excited photoabsorber and reducing agent or the solvent, which turns the photoabsorber into the radical anion. Then, Pt(IV) prodrug reduction occurs via single electron transfer (SET) from the axial radical anion to the Pt(IV) center; the light-induced decay of such Pt(IV) prodrugs is greatly accelerated in the presence of the reducing agent.[27]

The photoinduced decay of **GreenPt** complex was studied under low-dose green LED irradiation (530 nm, 6.5 mW/cm^2). In the absence of sodium ascorbate less than 20% of **GreenPt** complex was reduced after 1 hour of irradiation. When irradiated in the presence of 5 equivalents of sodium ascorbate, 75% of the complex was reduced within 2 minutes, followed by negligible decay for the next hour (Figure 1, C). Almost instantaneous reduction of the complex in the presence of the ascorbate strongly suggests that the light-induced decay of **GreenPt** complex occurs through the reaction of the triplet excited BODIPY with the ascorbate and the subsequent formation of the BODIPY radical anion (Figure 3). Since sodium ascorbate is the well-known ROS scavenger, we hypothesized the quenching of the reducing agent by the ROS formed in the solution.[42] Importantly, the light-induced decay of **GreenPt** was accompanied by the accumulation of cisplatin in the irradiated solution (Figure S28, SI).

Cyclic voltammetry. The validity of the photoinduced electron transfer (ΔG_0 PET) from the excited state of BODIPY to the Pt(IV) center was also verified by calculations of Gibbs free energy. For

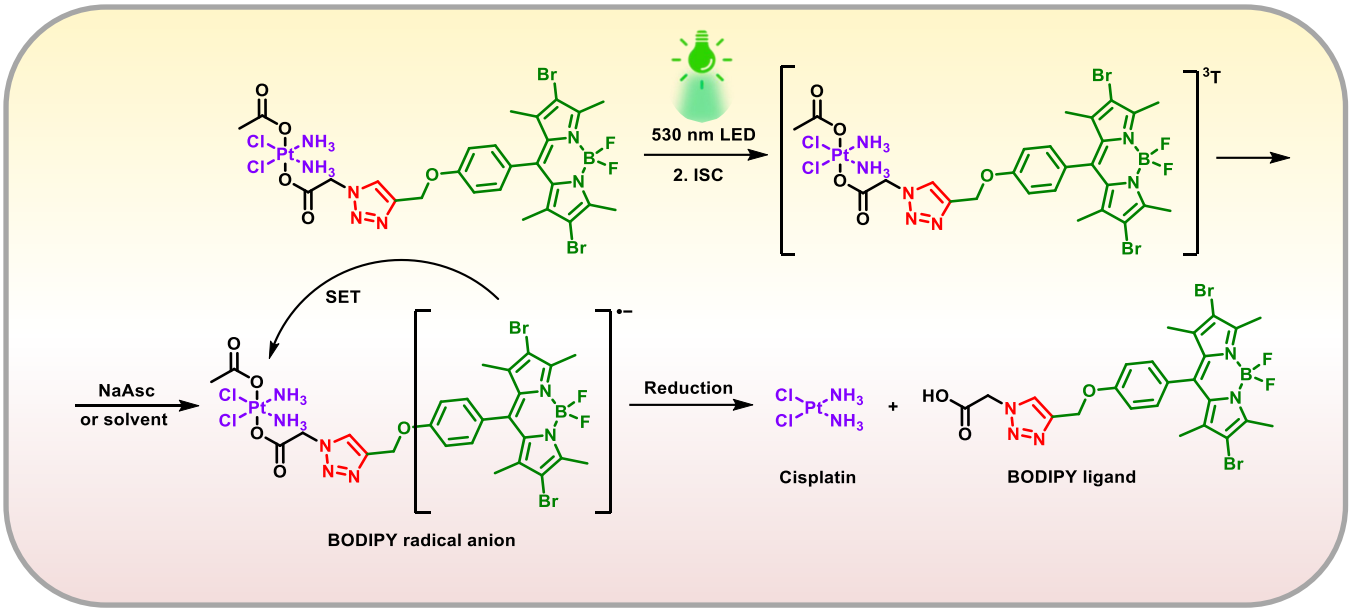

Figure 3. Proposed photoreduction mechanism of **GreenPt.** SET – single electron transfer.

this, redox behaviour of **GreenPt**, BODIPY **5** and **6** was estimated via cyclic voltammetry and square-wave voltammetry. For BODIPY **5** and **6,** a reversible reduction peak at -1.4 V could be observed on CVA curves, which could reasonably be attributed to the one-electron reduction of BODIPY with the formation of radical anion BODIPY$^{\bullet-}$ (Figure 1, D, Figure S29, S30, SI).

Importantly, a similar reduction peak for **GreenPt** complex at 1.4 V is irreversible, thus indicating BODIPY$^{\bullet-}$ radical anion rapidly reacts with Pt(IV) center. In addition, an increase in cathodic current approaching the S-shaped i/E curve is a good indicator that the formation of BODIPY radical anion is accompanied by the additional catalytic process.[43]

Gibbs energy calculations for GreenPt photoreduction. Free Gibbs energy of **GreenPt** complex's photoreduction was estimated using the previously published approach (See Experimental Section for the detailed calculation).[26] Taking into account the drastically higher photoreduction speed in the presence of an electron donor, the calculations were performed for the two-step process of BODIPY axial ligand photoreduction by sodium ascorbate with the formation of BODIPY$^{\cdot-}$ radical anion and the subsequent SET to the Pt(IV) center. The ΔG^0_{PET}value was obtained using the Rehm-Weller equation and was found to be -0.66 eV vs SHE. Considering that the first single-electron reduction that results in the formation of the unstable "Pt(III)" complex is the key step of Pt(IV) center reduction, for ΔG_{ET} calculation we utilized the E^0(Pt(IV)/Pt(III)) value -0.01 vs. SHE.[44] The resulting ΔG_{ET} value for the photoreduction of **GreenPt** complex from the triplet excited state was estimated to be -0.64 eV, thus confirming that the process is thermodynamically possible.

Thermodynamic DFT calculations also confirm the possibility of reduction of Pt(IV) from both ground and excited states of **reenPt** . Free Gibbs energies were computed for **GreenPt** in S_0, S_1 and T_1 states and ascorbate anion, as well as for reduction products, namely BODIPY, cisplatin, acetic acid, and dehydroascorbic acid following the previously reported procedure.[26] While $\Delta G°$ of -44.4 kcal/mol already favoures the reduction process of **GreenPt** from the ground state, this value increased to -107.4 and -76.8 kcal/mol from S_1 and T_1 state respectively. These results are in line with the observed facilitation of **GreenPt** reduction upon photoexcitation.

Antiproliferative properties *in vitro*. Based on the high singlet oxygen quantum yield of **GreenPt** complex and its ability to rapidly release cisplatin under green light irradiation, **GreenPt** is considered as a double-action Pt(IV) PACT/PDT prodrug. Hence, the antiproliferative activity of **GreenPt** prodrug as well as BODIPYs **5** and **8** was investigated on Sk-Br-3 cells under light and dark conditions (Figure 4, S31, SI, Table 2).

Heavy-atom photosensitizers BODIPYs **5** and **8** demonstrated an extremely high PI of >1300 and nanomolar efficacy under mild irradiation conditions (1 J/cm^2). These IC_{50} and PI values are superior to clinically used photosensitizers, which are typically effective at submicromolar or even micromolar concentrations *in vitro*.[45,46] Recently, a structurally similar series of dihalo-BODIPYs were reported by Badon et al with IC_{50} 49 nm and PI >>32.[35] The PI values of highly efficient NIR photosensitizers summarized by Tian in 2021 were limited to 7, while IC_{50} values under NIR light reported by Yang in 2013 were in the micromolar or submicromolar range.[47,48] Also, recently reported BODIPY – etacrynic acid conjugate exhibited light-induced activity in the micromolar range with PI equal to 10.[49] Thus, the PI values of BODIPYs **5** and **8** are one of the highest reported to date for BODIPY-based PDT agents. The incredible phototoxicity of BODIPYs **5, 8** can be explained by a low energy gap between S_1 and T_1 (ΔEst) and the high SOC constant, that facilitate the formation of the T_1 state and drastically enhance the production of ROS.[50,51]

GreenPt prodrug based of **CDDP** and BODIPY **5** showed dark toxicity 19.46±1.35 μM, which is two times lower compared to **CDDP**, while under green-light irradiation its antiproliferative activity increased > 100-fold up to nanomolar range. It is worth mentioning that the majority of photoactivated Pt(IV) prodrugs

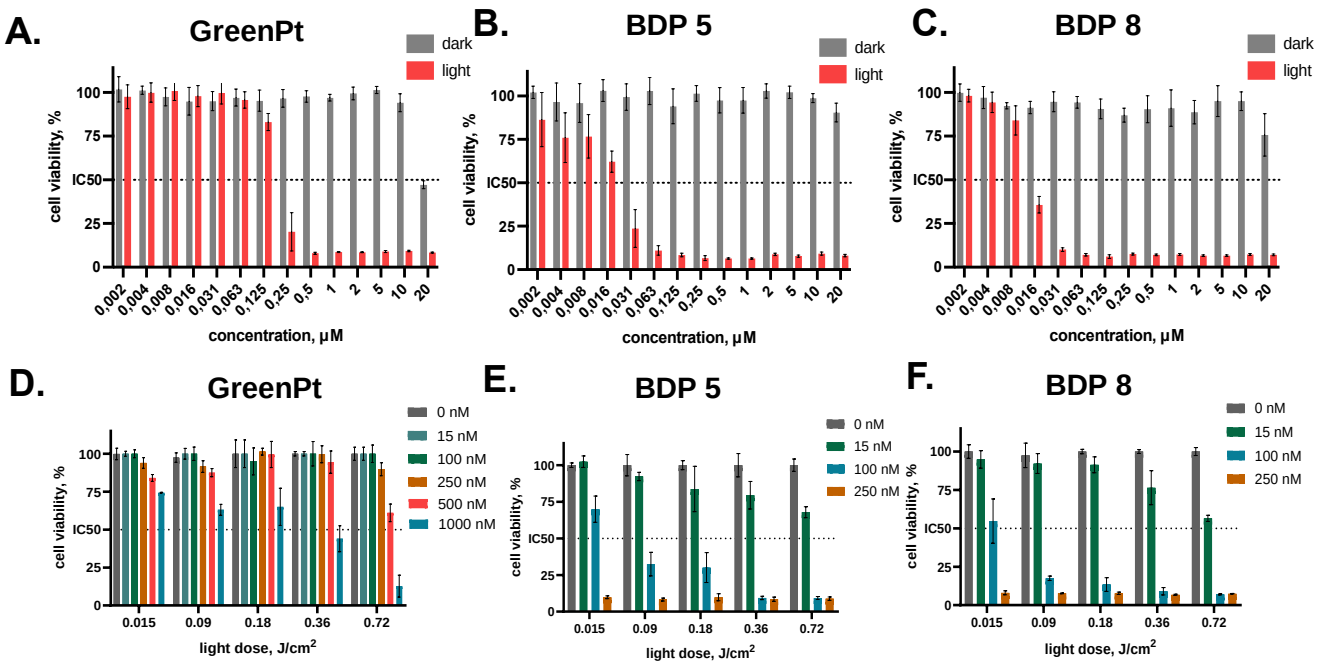

Figure 4. A - C. Cell viability curves of Sk-Br-3 cell line, incubated with (A) GreenPt Pt(IV) prodrug (B) BODIPY 5, or (C) 8 for 72 hours in the dark or irradiated with green LED (1 J/cm^2, 4 min 20 s) after 1.5 hours preindubation time. D - F. Cell viability curves of Sk-Br-3 cells, incubated with (D) GreenPt (E) BODIPY 5 or (F) 8 and irradiated with different green light doses (520 nm, 15-720 mJ/cm^2).

reported to date demonstrated only a mild increase in antiproliferative activity under light irradiation. In particular, activity of green-light activated BODIPY-Pt(IV) prodrug reported by Yao et al. increased only up to 11-fold after irradiation [28], and up to 5-fold increase in activity was observed for cyanine-conjugated cisplatin-based prodrug reported by Li et al.[52] Only two Pt(IV) prodrugs reported to date are superior to **GreenPt** in the light-induced response, namely Phorbiplatin, a double-action chemo/PDT Pt(IV) prodrug, and recently reported by Bera et al NIR-light activated BODIPY-based cisplatin prodrug.[26,31] However, aforementioned Pt(IV) prodrugs required high light doses in the range of 3.6 to 30 J/cm² for activation, which is significantly higher than the 1 J/cm² that required for **GreenPt**. We assume that **GreenPt**'s response to radiation is due to the incredible PDT activity of BODIPY **5**, which is released from it during irradiation.

Also, the irradiation dose-dependent phototoxicity of BODIPYs **5**, **8** and **GreenPt** prodrug was evaluated. Sk-Br-3 cells were incubated with various concentrations of compounds for 1.5 hours and then irradiated with different doses (15 – 720 mJ/cm²) green light. **GreenPt** demonstrated light dose-dependent phototoxicity, with IC_{50} value 1 μM at irradiation dose 0.4-0.8 J/cm² green light, which is still an exceptionally low light dose compared to those required for similar prodrugs reported to date (Figure 4, D). BODIPYs **5** and **8** confirmed an extraordinary phototoxicity even under ultralow light doses 15 mJ/cm² and completely inhibited cell viability at concentration as low as 250 nM (Figure 4, E, F). This confirms the outstanding photosensitizing properties of BODIPYs **5** and **8**.

To confirm the photodynamic mechanism of cell death, as well as to differentiate the actions of PDT Type I and Type II, cell viability on the presence of BODIPYs, **GreenPt** and radical scavengers was assessed. D-mannitol was used as an inhibitor of type I reactions since it can act as a superoxide anion radical (O_2^-) and hydroxyl radical (HO•) scavenger. [53] The addition of 12.5 mM mannitol or histidine to cell media did not affect light-

Table 2. Human breast carcinoma Sk-Br-3 cell viability data (IC_{50} and PI values) after 72 h incubation with **GreenPt**, BODIPYs **5** and **8**, and CDDP (MTT assay).

Compound	IC_{50}, μM		
	Dark	Irradiation	PI*
GreenPt	19.46±1.35	0.184±0.013	~105
BODIPY **5**	> 20	0.0137±0.021	> 1500
BODIPY **8**	> 20	0.021	> 1300
CDDP	10.31±1.99	9.16±1.76	1.1

* PI, calculated as the ratio of IC_{50} value under irradiation to IC_{50} value in the dark

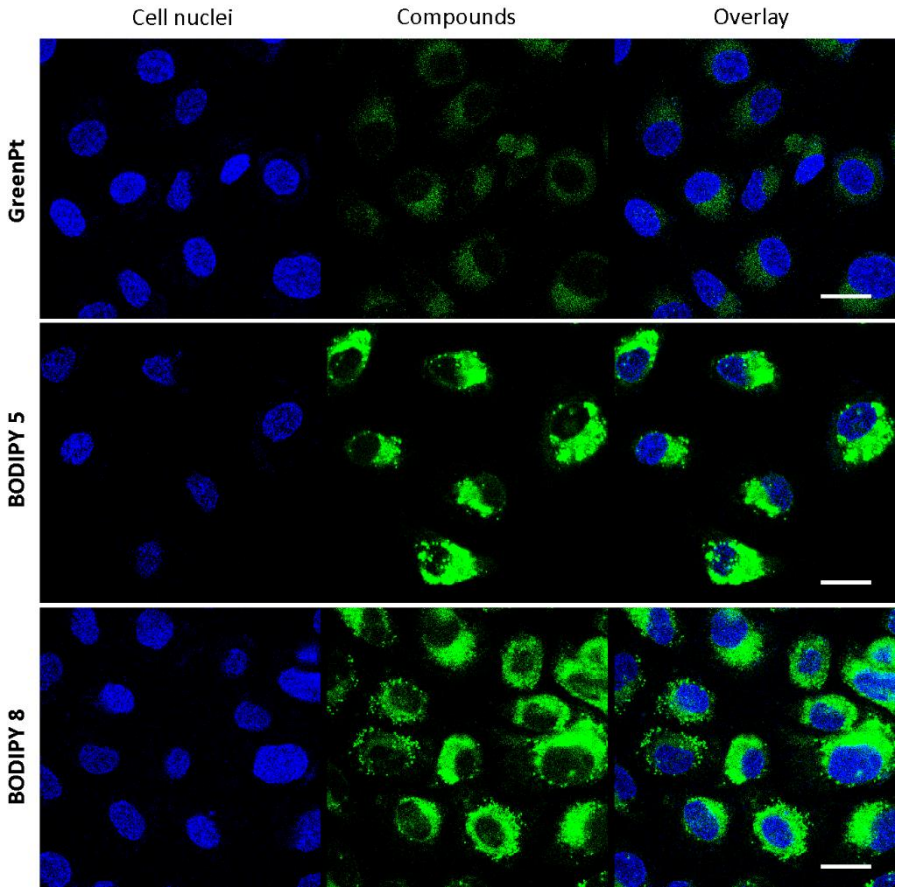

Figure 5. Intracellular accumulation of **GreenPt** and BODIPYs **5** and **8** in human breast cancer Sk-Br-3 cells, 10 µM, 30 min incubation. Cell nuclei were additionally stained with Hoechst 33342. Fluorescence was analysed at 405 nm (Hoechst 33342, in blue) and 488 nm (dyes, in green). Confocal microscopy data, scale-bar 20 µm.

induced cytotoxicity, thereby confirming that **GreenPt** does not act as a Type I PDT agent. However, the addition of 0.5 mM ascorbic acid to the cell medium as an antioxidant resulted in an increase in cell viability for **GreePt**-treated cells, suggesting that **GreenPt** acts as a Type II PDT agent (Figure S32, SI). [54]

Intracellular accumulation & distribution. We hypothesized that the differences in cytotoxicity BODIPYs and **GreenPt** could be explained by differences in intracellular accumulation. First, the internalization rate of BODIPYs **5**, **8** and **GreenPt** prodrug was evaluated using cell cytometry. BODIPYs **5** and **8** exhibited substantial intracellular accumulation even after 5 minutes of incubation with Sk-Br-3 cells. In contrast, **GreenPt** complex demonstrated gradual accumulation over a 4-hour timeframe, which might indicate that **GreenPt** complex and BODIPYs **5** and **8** are internalized via different mechanisms (Figure S33, SI). The rapid accumulation of BODIPYs **5** and **8** in the cell compared to the gradual accumulation of **GreenPt** explains well the difference in their cytotoxicity.

Also, confocal microscopy data confirmed an ability of **GreenPt** and BODIPYs to accumulate in cells (Figure 5), proving that the Pt(IV) prodrug is able to cross the cell membrane and release the cytotoxic Pt(II) complex intracellularly under the action of light or intercellular reductases. BODIPYs **5** and **8** accumulated significantly faster in cells when compared with **GreenPt**, which is in a good correspondence with cytometry data. It should also be also noted that **GreenPt** distributed homogeneously in the cytoplasm, whereas BODIPY dyes showed dot-like intracellular accumulation (Figure S34, SI), which could be explained by binding with cell organelles, e.g. mitochondria or lysosomes.

Antitumor efficiency of Pt(IV) prodrugs depends significantly on their resistance towards hydrolysis and reduction. Prodrugs that quickly release an active Pt(II) complex tend to degrade quickly in the bloodstream and thus their antitumor activity *in vivo* is almost indistinguishable to that of cisplatin.[14] In addition, several recently reported Pt(IV) prodrugs that demonstrated promising results *in vivo* were characterized by long bloodstream circulation time and gradual accumulation in tumor tissues.[55,56] Since **GreenPt** Pt(IV) prodrug demonstrated gradual accumulation in tumor cells and high stability towards reduction, it can be expected that the **GreenPt** would be gradually internalized by tumor tissues *in vivo*.

Conclusions

We have designed, synthesized and studied a novel dual-action Pt(IV) prodrug **GreenPt** with an efficient BODIPY-based photosensitizer in axial position, capable of both cisplatin release and ROS generation under low-dose green light irradiation. Pt(IV) prodrug with triplet photosensitizer based on BODIPY in the axial position was obtained for the first time via

a click reaction. **GreenPt** showed high stability to reduction, the ability to release e cisplatin under low dose green light irradiation; as well as a high quantum yield of singlet oxygen due to the presence of BODIPY **5** with outstanding PDT activity in the axial position. **GreenPt** demonstrated gradual intracellular accumulation, along with a PI> 100, which is higher than that of for most photoactivatable Pt(IV) prodrugs published to date, thus demonstrating its high potential as a photoactivatable PACT/PDT prodrug. BODIPYs **5** and **8** demonstrated outstanding PDT activity *in vitro* with ultralow IC_{50} values after low-dose (1 J/cm^2) irradiation with PI>1300 and were capable of inhibiting cell viability even after ultra-low-dose irradiation of 15 mJ/cm^2. A photoreduction mechanism of **GreenPt** prodrug was proposed based on DFT modeling and ΔG_0 PET estimation, an anion-radical formation and photoinduced electron transfer from the triplet excited state of the BODIPY axial ligand to the Pt(IV) center was proposed as the key step.

In summary, we have demonstrated how conjugation of clinically used Pt(II) drug with the highly potent photosensitizers could lead to the light-activated antitumor agent that is stable low-toxic in the dark but could be activated with low-dose green light, leading to drastic increase in antiproliferative activity. The obtained results will pave the way for the development of safe yet highly effective Pt-based drugs and PDT agents.

Experimental

Materials and Methods

Acetic acid, acetoacetic ester, ammonium hydroxide (NH_4OH), 2-azidoacetic acid, boron trifluoride etherate ($BF_3{\cdot}Et_2O$), cisplatin, copper sulfate pentahydrate ($CuSO_4{\cdot}5H_2O$), diisopropylethyl amine (DIPEA), 2,3-dichloride- 5,6-dicyano-p-benzoquinone (DDQ), N,N'-dicyclohexylcarbodiimide (DCC), ethylene glycol, hydrogen peroxide (30% w/w in water), 4-hydroxybenzaldehyde, N-bromosuccinimide (NBS), propargyl bromide, potassium carbonate (K_2CO_3), potassium hydroxide (KOH), sodium azide (NaN_3), sodium ascorbate, sodium bicarbonate ($NaHCO_3$), sodium nitrite ($NaNO_2$), trifluoroacetic acid (TFA), triethylamine(Et_3N), zinc powder (Aldrich, Alfa, AKSci, etc.) were used without purification. Acetone, acetonitrile (CH_3CN), dichloromethane (DCM, CH_2Cl_2), diethyl ether (Et_2O), ethyl acetate (EtOAc), methanol (MeOH), dimethylformamide (DMF), dimethyl sulfoxide (DMSO) and petroleum ether were purchased from commercial sources and purified following the described procedures.[57]

IR spectra were measured on a TermoNicolet IR 200 Fourier spectrometer (Termo Scientific, Waltham, MA, USA; resolution 4 cm^{-1}).

Analytical thin-layer chromatography (TLC) was performed on Merck silica gel aluminum plates with F-254 indicator. Compounds were visualized by irradiation with UV light (254, 365 nm).

Preparative column chromatography was performed using Acros brand silica gel (60–200 mesh).

NMR spectra were recorded on a Bruker Avance 400 MHz spectrometer (USA) in DMSO-d_6 and $CDCl_3$ with TMS as an internal standard for ^{1}H and ^{13}C and K_2PtCl_6 for ^{195}Pt NMR. All ^{13}C spectra were ^{1}H decoupled.

High-resolution mass spectra (HRMS) were recorded with a Xevo G3 QTof (quadrupole-time-of-flight mass spectrometer Waters, USA) equipped with an electrospray ionization (ESI). Conditions were as follow: resolution mode; capillary voltage 1,5 kV for positive polarity and -1kV for negative polarity, sampling cone 30, source offset 40; source and desolvation temperatures were 120 °C and 450 °C,respectively; cone gas flow 50 L/h and desolvation gas flow 700 L/h. The mass spectrometer was calibrated with the tuning solutions according to the manufacturer's recommendations prior to analysis. MassLynx software (version 4.2, Waters, USA) was used to acquire and process MS data. Mass-spectra were recorded in m/z range 150 – 3000.

Purity of the compounds was assessed using HPLC-DAD-MS. HPLC-DAD-MS system consisting of a Vanquish liquid chromatograph (Thermo Fisher Scientific, USA) and an Orbitrap Fusion Lumos Tribrid (Thermo Fisher Scientific, USA) mass spectrometer was used. A Shim-pack GIST C18-Aq liquid chromatography reversed-phase column (3 x 150 mm, 3 µm, Shimadzu, Japan) was used.

HPLC-HRMS analysis was performed with Vanquish liquid chromatograph (Thermo Fisher Scientific, USA) and a high-resolution mass spectrometer based on the Orbitrap Fusion Lumos Tribrid equipped with an electrospray ionization source (ESI) was used. To separate the components of the analyzed solution, a Shim-pack GIST C18-Aq chromatographic column (3 x 150 mm, 3 µm, Shimadzu, Japan) filled with a reverse-phase sorbent with polar-endcapping was used. The column temperature was maintained at 35 °C throughout the analysis using a thermostat. A 0.1% aqueous solution of formic acid (A) and acetonitrile (B) were used as eluents. An isocratic elution mode was used with a ratio of eluents A and B of 15:85%. The flow rate of the mobile phase was 0.4 mL/min. The injected sample volume was 1.0 µl. The analysis time was 10 minutes. The ESI-MS conditions on the Orbitrap Fusion Lumos Tribrid were as follows: mode for recording positively and negatively charged molecules; the capillary voltage of the ionization source was 3500 V for the positive mode and -2500 V for the negative mode; ion source chamber temperature - 350 °C; ion transfer interface temperature – 325 °C; gas pressure for solvent atomization in the ion source (nitrogen) - 50, auxiliary gas pressure - 10, curtain gas pressure - 1. Scanning range m/z: 200-1700 Da. The resolution of the mass spectrometer for analysis is not less than 15000. The mass spectrometer was calibrated immediately prior to sample analysis using CalMix PierceTM calibration mixtures (Thermo Scientific, USA). Data processing was performed using Xcalibur 4.6 software (Thermo Scientific, USA).

Cyclic and square wave voltammetry was performed at room temperature with the use of potentiostat/galvanostat PalmSens 3 (PalmSens, Netherlands). A three-electrode cell contained glassy carbon working (2.0 mm diameter) and auxiliary electrodes, and an

Ag/Ag+ reference electrode. The surface of glassy carbon electrodes in Teflon bodies were polished before each measurement using Al_2O_3 (10 and 0.05 µm) and wet microcloth pad in distill water. Between the individual polishing steps, the electrodes were rinsed with distilled water and dried. The electrochemical cell was filled with CH_2Cl_2 with dissolved tetrabutylammonium tetrafluoroborate (0.1 mol/L) as a supporting electrolyte. The working electrode compartment was filled with ligand or complex (2 mM) solution prepared in the same supporting electrolyte. Ferrocene was added as internal standard. Prior to the measurement the cell was purged with argon for 5-10 min.

Quantum-chemical calculations were performed in ORCA 6.0.0 package.[58,59] The analysis of computational results was performed using the Multiwfn 3.8(dev) [60] package. Geometry optimization was performed using the range-separated CAM-B3LYP functional with relativistic full-electron basis sets (ZORA-def2-TZVP for light elements and SARC-ZORA-TZVP for Pt) within relativistic ZORA approximation.[61,62] Solvation model based on density (SMD)[63] was applied with parameters for methanol.

Supplemental Experimental Procedures

Cytotoxicity study

IC_{50} determination

Human breast carcinoma Sk-Br-3 cells were seeded in 96-well plates (5×10^4 cells per well) in DMEM supplemented with 10% fetal bovine serum, 2 mM L-glutamine, and 1% solution of penicillin (100 U/mL) and streptomycin (100 µg/mL). The next day, the medium in each well was replaced with 100 mL of fresh DMEM containing test substances in the concentration range of 2 nM - 20 µM. Cells were incubated with the compounds for 2 hours followed by irradiation at a wavelength of 530 nm with a light dose of 1 J/cm^2; non-irradiated cells were used as control. Cell viability was assessed after 72 hours using the MTT assay. For this, MTT solution (0.5 mg/mL) was added to each well for 2 hours, then the medium was removed and 100 mL DMSO (99%) was added to dissolve the formazan crystals. Absorbance was recorded at 565 nm using an Infinite M Nano reader (Tecan, Switzerland). The IC_{50} values were determined using GraphPad Prism 8.0 software.

Light dose-dependent cytotoxicity

Human breast carcinoma Sk-Br-3 cells seeded in 96-well plates (5×10^4 cells per well) and incubated overnight were treated with 15 nM, 100 nM, and 250 nM for BODIPY dyes **5** and **8**, and with 15 nM, 100 nM, 250 nM, 400 nM, and 1000 nM for **GreenPt** complex. After 2 h incubation, cells were irradiated at a wavelength of 530 nm with a light dose of 0.015 to 0.72 J/cm^2; non-irradiated cells were used as control. Cell viability was assessed after 72 hours by the MTT assay as described above.

Antioxidants-dependent cytotoxicity

Human breast carcinoma Sk-Br-3 cells seeded in 96-well plates (5×10^4 cells per well) and incubated overnight were treated with 15 nM, 100 nM, and 250 nM for BODIPY dyes **5** and **8**, and with 250 nM, 400 nM, and 1000 nM for **GreenPt** complex. Additionally, 0.5 mM of ascorbic acid (Chimmed), 12.5 mM mannitol (Chimmed), or 2.5 mM histidine (Chimmed) were added to the medium as antioxidants. After 12 hours of incubation, the medium was changed to fresh medium and the cells were irradiated at a wavelength of 530 nm with a light dose of 0.72 J/cm^2; non-irradiated cells were used as control. Cell viability was assessed after 48 hours using the MTT assay as described above.

Flow cytometry

Human breast carcinoma Sk-Br-3 cells were plated on 6-well plates (10^6 cells per well) and incubated overnight. Then, 10 µM of **GreenPt** complex or BODIPY days were added to the cells in full DMEM media for 5 min - 4 h, after which the cells were washed in phosphate buffer and detached with trypsin solution (0.25%). Fluorescence was measured on a channel corresponding to FITC fluorescence and at least 20,000 events were examined for each sample.

Confocal microscopy

Human breast carcinoma Sk-Br-3 cells were plated on 8-well microscope slide flasks (10^5 cells per well) and incubated overnight. Then, 10 µM of **GreenPt** complex or BODIPY days were added to the cells in complete DMEM medium for 30 minutes, after which the medium was replaced and the cells were irradiated at a wavelength of 530 nm, 1 J/cm^2. The cells were then washed in phosphate buffer to remove unbound substances and fixed in 4% paraformaldehyde. The nuclei were additionally stained with 10 µM Hoechst 33342. Fluorescence was analyzed at wavelengths of 405 nm (Hoechst 33342), and 488 nm and 543 nm (dyes) using a Leica TSP SPE confocal laser scanning system (Leica, Germany).

Gibbs free energy of photoinduced electron transfer evaluation

The validity of the proposed mechanism was proved by calculations of ΔG^0_{PET} of photoinduced electron transfer (PET) from ascorbate to the excited BODIPY:

$$\Delta G^0_{PET} = -F(E_{1/2}(\mathbf{Pt}\ /\ \mathbf{Pt^{-\bullet}}) - E_{1/2}(\mathrm{NaAsc^{+\bullet}/NaAsc})) - E^*_{0,0} + \Delta G_s + W\ ,$$

where $E_{1/2}$ (NaAsc$^{+\bullet}$/NaAsc) is the half-wave potential of the electron donor (ascorbate), $E_{1/2}$ (**Pt** / **Pt**$^{-\bullet}$) is the half-wave potential of the acceptor. $E^*_{0,0}$ is the zero-to-zero energy for BODIPY for PET from the excited state. ΔG_s is the Born solvation energy, and W is the coulomb work term. W is negligible, approximately 0.02 - 0.04 eV. If the reduction potential and $E^*_{0,0}$ were measured in the same solvent media, $\Delta G_s = 0$. F is the Faraday constant (F = 1e for calculating the energy in eV),

$E_{1/2}$ (NaAsc$^{+\bullet}$/NaAsc) = ~ 0.4V vs. SHE, according to literature.[64]

The singlet excited state energy $E^*_{0,0}$ was calculated from the emission band known for BODIPY using the equation:

$E^*_{0,0} = hc / \lambda_{max} = 1240\ nm / \lambda_{max} = 1.61\ eV$

$E_{1/2}$ (Pt-BODIPY / Pt-BODIPY$^{-\bullet}$) was obtained from its reduction peak on the SWV (Figure S29).

For the electron transfer from BODIPY$^{-\bullet}$ to Pt(IV), the free energy was estimated using equation:

$\Delta G_{ET} = -F(E_0(\text{Pt (IV) / Pt(III)}) - E_{1/2}$ (**Pt / Pt$^{-\bullet}$**)

E^0(Pt (IV)/Pt (III)) =~ -0.01 vs. SHE, according to literature for $Pt^{IV}(NH_3)_2Cl_2(OAc)_2$ we use -0.02 V in our calculation.

$E_{1/2}$ (**Pt / Pt$^{-\bullet}$**) = -1.35 V vs. Ag/Ag$^+$ = -0.55 V vs. SHE

1) ΔG^0_{PET} = 0.40 – (-0.55) – 1.61= -0.66 eV

2) ΔG_{ET} = -0.66 – (-0.02) = -0.64 eV

Stability and photoreduction studies

All experiments were carried out at room temperature. Complex **GreenPt** was dissolved in a mixture of MeOH:DMSO:H_2O (14:5:1) to the resulting concentration of 10^{-3} M. In the experiments carried out under reductive conditions, the mixture solution was supplemented with the sodium ascorbate. The **GreenPt** solution was placed in the dark for the experiments without irradiation. In the experiments with light activation, the **GreenPt** solution in a transparent vial (d = 1 cm) was placed in front of the light source (λ = 530 nm) so that irradiation power density was equal to 6.5 mW/cm^2.
In all experiments a 30 μl aliquot of the Pt(IV) prodrugs solution was taken and diluted 16 times with MeOH at the chosen periods of time. HPLC-MS-analysis of the probes was performed and repeated three times. **GreenPt** and cisplatin amount in the probes were calculated from the peak area on the chromatogram. Cisplatin concentration was determined by integrating m/z 340.5-345.5 Da peak, which corresponds to $Pt(NH_3)_2Cl(C_2H_6SO)$ ion; concentration of **GreenPt** complex was determined by integrating m/z 991.9761 Da peak.

Synthetic procedures

Diethyl 3,5-dimethyl-1*H*-pyrrole-2,4-dicarboxylate 1. The synthesis was performed following the previously published procedure with slight modifications.[65] To a mixture of acetoacetic ester (30 mL, 0.24 mol) and acetic acid (60 mL), a solution of $NaNO_2$ (8.20 g, 0.12 mol) in 12 mL of water was added dropwise over 30 minutes while keeping the temperature of the reaction mixture below 10 °C. The solution was stirred at 10 °C for 2.5 hours. Zinc dust (15.4 g, 0.240 mol) was then added in portions to the reaction mixture while keeping the temperature of the reaction mixture not higher than 25 °C. The reaction mixture was then gradually heated to 40-50 °C , stirred at this temperature for ~10 minutes and then gradually heated to 95 °C. After complete dissolution of the precipitate, the reaction mixture was stirred at 95-100 °C for ~1 hour and then quickly poured into 150-200 mL of water without allowing the reaction to cool. The precipitate was filtered, washed with cold water and then with cold ethanol. 48 g of diethyl 3,5-dimethyl-1H-pyrrole-2,4-dicarboxylate **1** was obtained in the form of a light beige powder. Yield: 18 g (56 %).

^{1}H NMR (400 MHz, $CDCl_3$, δ, ppm): 8.89 (br. s, 1H, NH, H-e), 4.39 – 4.23 (m, 4H, $O\underline{CH_2}CH_3$, H-b), 2.56 (s, 3H, CH_3, H-d), 2.51 (s, 3H, CH_3, H-c), 1.39 – 1.33 (m, 6H, $OCH_2\underline{CH_3}$, H-a).

^{13}C NMR (101 MHz, $CDCl_3$, δ, ppm): 165.68, 162.13, 139.34, 131.14, 118.03, 113.64, 60.50, 59.63, 14.55, 14.53, 14.41, 12.14.

2,4-dimethyl-1*H*-pyrrole 2. Pyrrole **2** was synthesized according to previous reports procedure with slight modifications.[66] A mixture of diethyl 3,5-dimethyl-1*H*-pyrrole -2,4-dicarboxylate **1** (30 g, 0,14 mol) and KOH (40.6 g, 0.72 mol) in 100 mL of ethylene glycol was refluxed for 4 hour at 160°C. Then, the solution was cooled to room temperature and 200 mL of brine was added. The product was extracted with CH_2Cl_2 (3x300 mL), dried with anhydrous Na_2SO_4 and then concentrated. The crude product was distilled in vacuum, T_B = 65-70°C (12-14 mm Hg). Pyrrole **2** was obtained as a transparent colorless liquid and was stored under Ar and -20°C. Yield: 3.8 g (32%).

^{1}H NMR (400 MHz, $CDCl_3$, δ, ppm): 7.61 (br. s, 1H, NH, H-e), 6.41 (s, 1H, 5-CH, H-d), 5.74(s, 1H, 2-CH, H-b), 2.23 (s, 3H, 2-CH_3, H-a), 2.07 (s, 3H, 4-CH_3, H-c).

^{13}C NMR (101 MHz, $CDCl_3$, δ, ppm): 127.83, 119.22, 113.92, 107.73, 13.10, 11.99

4-(5,5-difluoro-1,3,7,9-tetramethyl-5*H*-4λ^4,5λ^4-dipyrrolo[1,2-*c*:2',1'-*f*][1,3,2]diazaborinin-10-yl)phenol) **3**. BODIPY **3** was synthesized according to previous reports procedure with slight modifications.[33] To a solution of 1 g (8.19 mmol, 1 equiv.) of 4-hydroxybenzaldehyde and 1.85 mL (18 mmol, 2.2 equiv.) of 2,4-dimethylpyrrole **2** in 150 mL of THF several drops of trifluoroacetic acid were added under an argon atmosphere. The mixture was stirred at r.t. for 6 hours, and the solution of 2.05 g (9.0 mmol, 1.1 equiv.) of DDQ in 100 mL of THF was added. The resulting mixture was stirred for another 5 hours. Then, the reaction mixture was cooled with an ice-water bath, then 25 mL of Et_3N and 31 mL of $BF_3{\cdot}Et_2O$ were added dropwise. The resulting mixture was kept stirring at r.t. overnight, then it was filtered through a band of silica gel. The precipitate was washed with CH_2Cl_2 and the combined filtrate was evaporated under reduced pressure. The residue was redissolved in CH_2Cl_2 and the solution was washed with 15% aqueous $NaHCO_3$ solution and with water. The organic layer was dried over anhydrous Na_2SO_4 and evaporated under reduced pressure. The crude product was purified by flash-chromatography using CH_2Cl_2 as eluent. BODIPY **3** was obtained as an orange powder. Yield: 1.9 g (74%).

^{1}H NMR (400 MHz, $CDCl_3$, δ, ppm): 7.13 (d, 2H, J=8.4 Hz, 2,6-Ph), 6.95 (d, 2H, J=8.5 Hz, 3,5-Ph), 5.98 (s, 2H, 2,6-BP), 4.96 (s, 1H, OH, H-a), 2.55 (s, 6H, 3,5-BP-CH_3), 1.44 (s, 6H, 1,7-BP-CH_3).

^{13}C NMR (101 MHz, $CDCl_3$, δ, ppm): 156.53, 155.47, 143.34, 141.95, 131.99, 129.56, 127.32, 121.30, 116.27, 14.69.

5,5-difluoro-1,3,7,9-tetramethyl-10-(4-(prop-2-yn-1-yloxy)phenyl)-5*H*-4λ^4,5λ^4-dipyrrolo[1,2-*c*:2',1'-*f*][1,3,2]diazaborinine 4. BODIPY **4** was synthesized according to previous reports procedure with slight

modifications.[67] 200 mg (0.59 mmol, 1 equiv.) of BODIPY **3**, 261 μl (2.94 mmol, 5 equiv., 80% w/t in toluene) of propargyl bromide, and 408 mg (2.95 mmol, 5 equiv.) of K_2CO_3 were dissolved in 12 mL of acetone. The reaction mixture was refluxed for 2 hours. Then, the solvent was evaporated under reduced pressure. The crude product was purified by flash chromatography using CH_2Cl_2 as eluent. BODIPY **4** was obtained as a bright red powder. Yield: 213 mg (98%).

^{1}H NMR (400 MHz, $CDCl_3$, δ, ppm): 7.20 (d, 2H, J=8.6 Hz, 2,6-Ph), 7.09 (d, 2H, J=8.7 Hz, 3,5-Ph), 5.98 (s, 2H, 2,6-BP), 4.76 (d, 2H, J=1.8 Hz, O$\underline{CH_2}$C≡CH, H-a), 2.59-2.52 (m, 7H, 3,5-BP-CH_3, OCH_2C≡$\underline{CH}$, H-b), 1.42 (s, 6H, 1,7-BP-CH_3).

^{13}C NMR (101 MHz, DMSO, δ, ppm): 157.82, 154.71, 142.75, 141.95, 131.07, 129.11, 126.68, 121.31, 115.64, 78.89, 78.52, 55.68, 14.22, 14.15.

HRMS: calc. for $C_{22}H_{22}BF_2N_2O^+$ 379.1793 (**4**+H)$^+$; found $C_{22}H_{22}BF_2N_2O^+$ 379.1782 (**4**+H)$^+$.

2,8-dibromo-5,5-difluoro-1,3,7,9-tetramethyl-10-(4-(prop-2-yn-1-yloxy)phenyl)-5*H*-4λ^4,5λ^4-dipyrrolo[1,2-c:2',1'-*f*][1,3,2]diazaborinine 5. 283 mg (0.75 mmol, 1 equiv.) of BODIPY **4**, 333 mg (1.87 mmol, 2.5 equiv.) of N-Bromosuccinimide (NBS) were dissolved in 18 mL of CH_2Cl_2. The mixture was stirred at r.t. in the dark for 3.5 hours. Then, the solvent was evaporated under reduced pressure. The crude product was purified by flash chromatography using CH_2Cl_2: petroleum ether = 2:1 as eluent. BODIPY **5** was obtained as a dark red powder. Yield: 365 mg (91%).

^{1}H NMR (400 MHz, $CDCl_3$, δ, ppm): 7.27 (d, 2H, J=8.7 Hz, 2,6-Ph), 7.12 (d, 2H, J=8.8 Hz, 3,5-Ph), 4.78 (d, 2H, J=2.5 Hz, O$\underline{CH_2}$C≡CH, H-a), 2.60 (s, 6H, 3,5-BP-CH_3), 2.57 (t, 1H, J = 2.4 Hz, OCH_2C≡$\underline{CH}$, H-b), 1.42 (s, 6H, 1,7-BP-CH_3).

^{13}C NMR (101 MHz, DMSO-d_6, δ, ppm): 158.59, 154.00, 140.75, 130.86, 129.25, 127.41, 116.06, 77.97, 76.23, 56.19, 14.02, 13.83.

[OC-6-44]-Acetatodiammineddichloridohydroxidoplatinum(IV) 6. Compound **6** was synthesized according to previous reports.[68] 100 mg (0.334 mmol) of cisplatin was dissolved in 40 mL of glacial acetic acid and 1.7 mL of H_2O_2 (30% w/w) was added. The reaction mixture was stirred for 1.5 hours at 35–40°C until the precipitate dissolved and the solution became transparent. Then, the solution was concentrated under reduced pressure until the volume of the mixture is reduced to ~ 3 mL. The excess (30 mL) of diethyl ether was added and the resulting suspension was centrifuged. The precipitate was separated and washed with diethyl ether, then air-dried. Compound **6** was obtained as a white powder. Yield: 119 mg (95%).

^{1}H NMR (400 MHz, DMSO-d_6, δ, ppm.): 6.13 – 5.78 (m, 6H, NH_3), 1.87 (s, 3H, CH_3)

[Pt(OAc)(2-azidoacetate)(Cl_2(NH_3)$_2$)] 7. The synthesis was performed following the previously published procedure with slight modifications.[69] 266 mg (1.29 mmol, 4 equiv.) of DCC was dissolved in 6 mL of DMF and 130 mg (1.29 mmol, 4 equiv.) of 2-azidoacetic acid was added. The reaction mixture was suspended in an ultrasonic bath for 15 min. Then, the formed precipitate was separated by centrifugation. The resulting solution of 2-azidoacetic anhydride in DMF was mixed with suspension of 121 mg (0.32 mmol, 1 equiv.) of compound **7** in 4.5 mL of DMF. The reaction mixture was stirred at 40 °C for 4 hours, then the solvent was removed under reduced pressure (the water bath temperature was kept under 45°C). The residue was purified by flash chromatography using EtOAc:MeOH = 5:1 as eluent. Compound **7** was obtained as a light-yellow powder. Yield: 98 mg (66%).

^{1}H NMR (400 MHz, DMSO-d_6, δ, ppm.): 6.88 – 6.20 (m, 6H, NH_3), 3.89 (s, 2H, C(O)CH_2N_3), 1.92 (s, 3H, C(O)-CH_3).

HRMS: calc. for $C_4H_{11}Cl_2N_5NaO_4Pt^+$ 480.9734 (**7**+Na)$^+$; found $C_4H_{11}Cl_2N_5NaO_4Pt^+$ 480.9735 (**7**+Na)$^+$.

GreenPt. 21 mg (0.039 mmol, 1.2 equiv.) of BODIPY **5** was dissolved in 1.5 mL of DMF and 3.1 mg (9.8 μmol, 0.3 equiv.) of Cu(CH_3CN)$_4$•BF_4 **10**, 5.2 mg (9.8 μmol, 0.3 equiv.) of TBTA **13** were added under argon atmosphere. The reaction mixture was stirred for 15 min at r.t., then 8 mg (0.033 mmol, 1 equiv.) of [Pt(OAc)(2-azidoacetate)(Cl_2(NH_3)$_2$)] **7** was added, and the solution was stirred for another 1 hour at r.t. The solvent was evaporated under reduced pressure. The residue was purified twice by column chromatography using CH_2Cl_2:MeOH = 10:1 and EtOAc:MeOH=5:1 as eluents. Complex **Pt-1** was obtained as a dark red powder. Yield: 9 mg (28%).

^{1}H NMR (400 MHz, DMSO-d_6, δ, ppm.): 8.18 (s, 1H, C=$\underline{CH}$-N), 7.35 (d, 2H, *J* = 8.8 Hz, 2,6-Ph), 7.286(d, 2H, *J* = 8.7 Hz, 3,5-Ph), 7.08 (d, *J* = 8.6 Hz, 4H, 3,5-Ph', H-g), 6.53 (br. s, 6H, NH_3), 5.24 (s, 2H, CO$\underline{CH_2}$N), 5.23 (s, 2H, O$\underline{CH_2}$, H-a), 2.52 (s, 6H, 3,5-BP-CH_3), 1.93 (s, 3H, C(O)CH_3), 1.41 (s, 6H, 1,7-BP-CH_3).

^{13}C NMR (101 MHz, DMSO-d_6, δ, ppm): 178.08, 173.32, 159.21, 152.88, 143.16, 141.99, 140.44, 130.27, 129.23, 126.12, 125.51, 115.64, 111.11, 61.29, 50.56, 40.20, 40.15, 39.99, 39.94, 39.83, 39.78, 39.73, 39.62, 39.57, 39.52, 39.41, 39.36, 39.31, 39.10, 38.89, 22.63, 13.62, 13.40.

^{195}Pt NMR (86 MHz, DMSO-d_6, δ, ppm): 1230.21

HRMS: calc. for $C_{26}H_{30}BBr_2Cl_2F_2N_7O_5Pt^+$ 995.9711 (**GreenPt**)$^+$; found $C_{26}H_{30}BBr_2Cl_2F_2N_7O_5Pt^+$ 995.9770 (**GreenPt**)$^+$.

Methyl 2-(4-((4-(2,8-dibromo-5,5-difluoro-1,3,7,9-tetramethyl-5*H*-4λ^4,5λ^4-dipyrrolo[1,2-c:2',1'-f][1,3,2]diazaborinin-10-yl)phenoxy)methyl)-1*H*-1,2,3-triazol-1-yl)acetate 8. 20 mg (0.04 mmol, 1 equiv.) of BODIPY **5** and 11.8 mg of methyl 2-azidoacetate (0.103 mmol, 2.8 equiv.) were dissolved in 6 mL of CH_2Cl_2 and 6 mg (0.02 mmol, 0.5 equiv.) of Cu(CH_3CN)$_4$•BF_4 **10** was added under argon atmosphere. The reaction mixture was stirred for 2 hours at r.t. The solvent was evaporated under reduced pressure and the residue was purified by flash chromatography using CH_2Cl_2: MeOH = 5:1 as eluent. BODIPY **6** was obtained as a dark red powder. Yield: 21 mg (86 %).

^{1}H NMR (400 MHz, $CDCl_3$) δ 7.83 (s, 1H, C=CH-N), 7.17 (d, 2H, *J* = 8.6 Hz, 2,6-Ph), 7.14 (d, 2H, *J* = 8.9 Hz, 3,5-Ph), 5.30 (s, 2H, $COCH_2N$), 5.23 (s, 2H, OCH_2, H-a), 3.84 (s, 3H, $COOCH_3$), 2.60 (s, 6H, 3,5-BP-CH_3), 1.41 (s, 6H, 1,7-BP-CH_3).

Copper oxide (I) 9. Cu_2O **9** was synthesized according to previous reports.[70] 5 g of $CuSO_4{\cdot}5H_2O$ (20 mmol, 2 equiv.) was added to 30 mL of aqueous solution containing 2.9 g (10 mmol, 1 equiv.) of EDTA and stirred for 30 min at 55 °C. Subsequently, 250 mL of NaOH solution (0.6 M) and 5.6 g (28 mmol, 2.8 equiv.) of sodium ascorbate were added into the above solution successively under stirring until the solution was cooled to room temperature, which resulted in a brick-red suspension. The precipitation was collected by centrifugation at 2000 rpm for 3 min and washed several times with deionized water and ethanol. After that, the precipitate was dried in a vacuum oven for 6 hours at 50 °C. Cu_2O **9** was obtained as an orange powder. Yield: 2.88 g (95%).

Tetrakis(acetonitrile)copper(I) tetrafluoroborate 10. $Cu(CH_3CN)_4{\bullet}BF_4$ **10** was synthesized according to previous reports.[71] To a stirred suspension of 2.9 g (20 mmol) of Cu_2O **9** in 58 mL of CH_3CN 9.5 mL of 48-50% HBF_4 were added in 1 mL portions. The reaction was exothermic. After the addition of the final portion of HBF_4, the solution was stirred for about 5 minutes and hot-filtered to remove undissolved solids. An equal volume of diethyl ether was then added to the filtrate and cooled to 0 °C for 2 hours, whereupon a white microcrystalline solid was formed. The solid was collected by filtration under reduced pressure, washed with diethyl ether and was dried under vacuum afterwards immediately. $Cu(CH_3CN)_4BF_4$ **10** was obtained as white crystals. Yield: 10.4 g (84%).

Azidomethylbenzene 11. The synthesis was performed following the previously published procedure with slight modification.[72] To a stirred solution of 3.5 g of (bromomethyl)benzene (0.02mmol, 1 equiv) in 0.82 mL of THF 2 g of NaN_3 (0.03 mmol, 1.5 eq) in 4 mL of water was added. The resulting suspension was refluxed for 3 hours. The mixture was extracted with CH_2Cl_2, washed with water, and filtered. The solvent was evaporated under reduced pressure. Azidomethylbenzene **11** was obtained as colorless liquid. Yield: 2.28 g (93%).

^{1}H NMR (400 MHz, CDCl3, δ, ppm): 7.44 – 7.28 (m, 5H, Ar-CH), 4.34 (s, 2H, CH_2).

Tri(prop-2-yn-1-yl)amine 12. Tripropargyl amine **12** was synthesized according to previous reports with slight modifications.[73] 7 mL (81.2 mmol, 1 equiv.) of propargyl bromide was added dropwise to 17 mL (110 mmol, 1.35 equiv.) of an aqueous solution of NH_4OH (25% w/w) within 3 hours. A color change to yellow as well as the precipitation of ammonium bromide could be observed, during stirring the mixture at r.t. for 24 hours. Afterwards, the reaction mixture was stirred at 50 °C for another 48 hours. The product was extracted with diethyl ether (3×10 mL) and dried with anhydrous Na_2SO_4. The solvent was evaporated under reduced pressure and the crude product was purified by column chromatography using Et_2O:petroleum ether = 1:1 as eluent. Tripropargyl amine **12** was obtained as colorless liquid. Yield: 1.9 g (54%).

^{1}H NMR (400 MHz, CDCl3, δ, ppm): 3.45 (d, 6H, J=2.4 Hz, NCH_2), 2.24 (t, 3H, J=2.4 Hz, C≡CH).

Tris[(1-benzyl-1H-1,2,3-triazol-4-yl)methyl]amine (TBTA) 13. TBTA **13** was synthesized according to previous reports.[74] 2.5 g of benzyl azide (6.0 mmol, 3.0 equiv.) **15** and 800 mg (2.01 mmol, 1 equiv.) of tripropargyl amine **12** were dissolved in 30 mL of CH_2Cl_2, and 30 mL of H_2O was added. Then, 76 mg (0.3 mmol, 0.15 equiv.) of $CuSO_4{\cdot}5H_2O$ and 180 mg (0.90 mmol, 0.45 equiv.) of sodium ascorbate were added and the reaction mixture was vigorously stirred over night at r.t. Then, 40 mL of CH_2Cl_2 and 40 mL of H_2O were added, and the organic phase was separated. The aqueous phase was extracted with CH_2Cl_2 (3×40 mL) and the combined organic phases were washed with 40 mL of brine and dried with anhydrous Na_2SO_4. The solvent was evaporated under reduced pressure and the crude product was purified by flash chromatography using CH_2Cl_2:MeOH 20:1 as eluent. TBTA **13** was obtained as a white powder. Yield: 2.7 mg (84%).

^{1}H NMR (400 MHz, $CDCl_3$, δ, ppm): 7.70 (s, 3H, C=CH-N, H-b), 7.42 – 7.23 (m, 15H, Ar-CH, H-Ph), 5.52 (s, 6H, Ph-CH_2, H-c), 3.73 (s, 6H, N-CH_2, H-a).

Author contributions

The manuscript was written through contributions of all authors. / All authors have given approval to the final version of the manuscript.

Conflicts of interest

There are no conflicts to declare.

Data availability

A data availability statement (DAS) is required to be submitted alongside all articles. Please read our full guidance on data availability statements for more details and examples of suitable statements you can use.

List of abbreviations

A549, adenocarcinomic human alveolar basal epithelial cells; Boc_2O, di-tert-butyl bicarbonate; CisPt (CDDP), cis-diamineplatinum(II) dichloride; DSC, N,N′-disuccinimidyl carbonate; DIPEA, N,N-diisopropylethylamine; DCM, di-cholоromethane; DMSO, dimethyl sulfoxide; DMF, N,N-dimethylformamide; DMEM, dulbecco's Modified Eagle Medium; DMEM/F12, dulbecco's Modified Eagle's Medium/Nutrient Mixture F-12 Ham; ESI, electrospray ionization; FBS, fetal bovine serum; HRMS, high-resolution mass spectrometry; HPLC, high-performance liquid chromatography; LC-

MS, liquid chromatography – mass spectrometry; HBSS, hanks' Balanced Salt solution; LED, light-emitting diode; MTT, 3-[4,5-dimethylthiazol-2yl]-2,5-diphenyl-tetrazolium bromide; NMR, nuclear magnetic resonance; PACT, photoactivated chemotherapy; PDT, photodynamic therapy; PET, photoinduced electron transfer; PS, photosentitizer; ROS, reactive oxygen species; SET, single electron transfer; SOC, spin–orbit coupling; TFA, trifluoroacetic acid; TLC, thin layer chromatography; TMS, tetramethylsilane; TCSPC, Time-Correlated Single Photon Counting; TBAP, tetrabutylammonium perchlorate.

Acknowledgements

MS studies were supported by Lomonosov Moscow State University Program of Development.
We thank Alexey Kostyukov, Anton Egorov and Mikhail Kuzmin for the study of triplet-triplet absorption of GreenPt and BODIPYs.

Funding Sources

This work was supported by the Russian Science Foundation, Grant No. 22-15-00182.
Cytotoxicity & confocal microscopy were supported as part of «Laser technologies for biomedical applications» (No. 122122600055-2) under the state order of the Ministry of Education of the Russian Federation.

Notes and references

1 D. Wang and S. J. Lippard, *Nat. Rev. Drug Discov.*, 2005, **4**, 307–320.
2 T. C. Johnstone, K. Suntharalingam and S. J. Lippard, *Philos. Trans. R. Soc. A Math. Phys. Eng. Sci.*, 2015, **373**, 20140185–20140185.
3 S. Rottenberg, C. Disler and P. Perego, *Nat. Rev. Cancer*, 2021, **21**, 37–50.
4 D. Resistance and I. S. Effects, 2011, 1351–1371.
5 R. Oun, Y. E. Moussa and N. J. Wheate, *Dalt. Trans.*, 2018, **47**, 6645–6653.
6 B. W. Harper, A. M. Krause-Heuer, M. P. Grant, M. Manohar, K. B. Garbutcheon-Singh and J. R. Aldrich-Wright, *Chem. – A Eur. J.*, 2010, **16**, 7064–7077.
7 V. Brabec and J. Kasparkova, *Drug Resist. Updat.*, 2002, **5**, 147–161.
8 L. Galluzzi, L. Senovilla, I. Vitale, J. Michels, I. Martins, O. Kepp, M. Castedo and G. Kroemer, *Oncogene*, 2012, **31**, 1869–1883.
9 T. C. Johnstone, K. Suntharalingam and S. J. Lippard, *Chem. Rev.*, 2016, **116**, 3436–3486.
10 M. Ravera, E. Gabano, M. J. McGlinchey and D. Osella, *Dalt. Trans.*, 2022, **51**, 2121–2134.
11 M. Ravera, E. Gabano, M. J. McGlinchey and D. Osella, *Inorganica Chim. Acta*, 2019, **492**, 32–47.
12 X. Li, Y. Liu and H. Tian, *Bioinorg. Chem. Appl.*, 2018, **2018**, 8276139.
13 C. Marotta, E. Giorgi, F. Binacchi, D. Cirri, C. Gabbiani and A. Pratesi, *Inorganica Chim. Acta*, 2023, **548**, 121388.
14 D. V. Spector, A. A. Bubley, E. K. Beloglazkina and O. O. Krasnovskaya, *Russ. Chem. Rev.*, 2023, **92**, 5096.
15 A. Kastner, I. Poetsch, J. Mayr, J. V. Burda, A. Roller, P. Heffeter, B. K. Keppler and C. R. Kowol, *Angew. Chemie - Int. Ed.*, 2019, **58**, 7464–7469.
16 D. Spector, K. Pavlov, E. Beloglazkina and O. Krasnovskaya, *Int. J. Mol. Sci.*, 2022, **23**, 14511.
17 J. Huang, W. Ding, X. Zhu, B. Li, F. Zeng, K. Wu, X. Wu and F. Wang, *Front. Chem.*, 2022, **10**, 876410.
18 N. Boens, B. Verbelen, M. J. Ortiz, L. Jiao and W. Dehaen, *Coord. Chem. Rev.*, 2019, **399**, 213024.
19 N. A. Bumagina, E. V. Antina, A. A. Ksenofontov, L. A. Antina, A. A. Kalyagin and M. B. Berezin, *Coord. Chem. Rev.*, 2022, **469**, 214684.
20 R. P. Sabatini, T. M. McCormick, T. Lazarides, K. C. Wilson, R. Eisenberg and D. W. McCamant, *J. Phys. Chem. Lett.*, 2011, **2**, 223–227.
21 J. Zhao, K. Xu, W. Yang, Z. Wang and F. Zhong, *Chem. Soc. Rev.*, 2015, **44**, 8904–8939.
22 J. Zou, Z. Yin, K. Ding, Q. Tang, J. Li, W. Si, J. Shao, Q. Zhang, W. Huang and X. Dong, *ACS Appl. Mater. Interfaces*, 2017, **9**, 32475–32481.
23 A. Kamkaew, S. H. Lim, H. B. Lee, L. V. Kiew, L. Y. Chung and K. Burgess, *Chem. Soc. Rev.*, 2013, **42**, 77–88.
24 J. J. Hu, Q. Lei and X. Z. Zhang, *Prog. Mater. Sci.*, 2020, **114**, 100685.
25 T. C. Pham, V. N. Nguyen, Y. Choi, S. Lee and J. Yoon, *Chem. Rev.*, 2021, **121**, 13454–13619.
26 Z. Wang, N. Wang, S. C. Cheng, K. Xu, Z. Deng, S. Chen, Z. Xu, K. Xie, M. K. Tse, P. Shi, H. Hirao, C. C. Ko and G. Zhu, *Chem*, 2019, **5**, 3151–3165.
27 O. O. Krasnovskaya, R. A. Akasov, D. V. Spector, K. G. Pavlov, A. A. Bubley, V. A. Kuzmin, A. A. Kostyukov, E. V. Khaydukov, E. V. Lopatukhina, A. S. Semkina, K. Y. Vlasova, S. A. Sypalov, A. S. Erofeev, P. V. Gorelkin, A. N. Vaneev, V. N. Nikitina, D. A. Skvortsov, D. A. Ipatova, D. M. Mazur, N. V. Zyk, D. A. Sakharov, A. G. Majouga and E. K. Beloglazkina, *ACS Appl. Mater. Interfaces*, 2023, **15**, 12882–12894.
28 H. Yao, S. Chen, Z. Deng, M. K. Tse, Y. Matsuda and G. Zhu, *Inorg. Chem.*, 2020, **59**, 11823–11833.
29 A. Bera, S. Gautam, M. K. Raza, P. Kondaiah and A. R. Chakravarty, *J. Inorg. Biochem.*, 2021, **223**, 111526.
30 D. Spector, A. Bubley, A. Zharova, V. Bykusov, D. Skvortsov, D. Ipatova, A. Erofeev, P. Gorelkin, A. Vaneev, D. Mazur, V. Nikitina, M. Melnikov, V. Pergushov, D. Bunin, V. Kuzmin, A. Kostyukov, A. Egorov, E. Beloglazkina, R. Akasov and O. Krasnovskaya, *ACS Appl. Bio Mater.*, 2024, **7**, 3431–3440.
31 A. Bera, S. Gautam, S. Sahoo, A. K. Pal, P. Kondaiah and A. R. Chakravarty, *RSC Med. Chem.*, 2022, **13**, 1526–1539.
32 A. Bera, A. Nepalia, A. Upadhyay, D. Kumar Saini and A. R. Chakravarty, *Dalt. Trans.*, 2023, **52**, 13339–13350.
33 J. Park, D. Feng and H.-C. Zhou, *J. Am. Chem. Soc.*, 2015, **137**, 1663–1672.
34 W. Hu, R. Zhang, X.-F. Zhang, J. Liu and L. Luo, *Spectrochim. Acta Part A Mol. Biomol. Spectrosc.*, 2022, **272**, 120965.
35 I. W. Badon, J.-P. Jee, T. P. Vales, C. Kim, S. Lee, J. Yang, S. K. Yang and H.-J. Kim, *Pharmaceutics*, 2023, **15**, 1512.

36 Z. Xu, Z. Wang, Z. Deng and G. Zhu, *Coord. Chem. Rev.*, 2021, **442**, 213991.
37 Z. Deng, N. Wang, Y. Liu, Z. Xu, Z. Wang, T.-C. Lau and G. Zhu, *J. Am. Chem. Soc.*, 2020, **142**, 7803–7812.
38 N. Graf and S. J. Lippard, *Adv. Drug Deliv. Rev.*, 2012, **64**, 993–1004.
39 D. Corinti, M. E. Crestoni, S. Fornarini, E. Dabbish, E. Sicilia, E. Gabano, E. Perin and D. Osella, *JBIC J. Biol. Inorg. Chem.*, 2020, **25**, 655–670.
40 J. Z. Zhang, E. Wexselblatt, T. W. Hambley and D. Gibson, *Chem. Commun.*, 2012, **48**, 847–849.
41 H. Sun, S. S. Yee, H. B. Gobeze, R. He, D. Martinez, A. L. Risinger and K. S. Schanze, *ACS Appl. Mater. Interfaces*, 2022, **14**, 15996–16005.
42 B. Liu, J. Jiao, W. Xu, M. Zhang, P. Cui, Z. Guo, Y. Deng, H. Chen and W. Sun, *Adv. Mater.*, 2021, **33**, 2100795.
43 B. Speiser, in *Encyclopedia of Electrochemistry*, Wiley, 2007.
44 M. C. McCormick, K. Keijzer, A. Polavarapu, F. A. Schultz and M.-H. Baik, *J. Am. Chem. Soc.*, 2014, **136**, 8992–9000.
45 M. Wawrzyńska, W. Kałas, D. Biały, E. Zioło, J. Arkowski, W. Mazurek and L. Strządała, *Arch. Immunol. Ther. Exp. (Warsz).*, 2010, **58**, 67–75.
46 M. O. Senge and J. C. Brandt, *Photochem. Photobiol.*, 2011, **87**, 1240–1296.
47 Y. Tian, Q. Cheng, H. Dang, H. Qian, C. Teng, K. Xie and L. Yan, *Dye. Pigment.*, 2021, **194**, 109611.
48 Y. Yang, Q. Guo, H. Chen, Z. Zhou, Z. Guo and Z. Shen, *Chem. Commun.*, 2013, **49**, 3940–3942.
49 M. Won, S. Koo, H. Li, J. L. Sessler, J. Y. Lee, A. Sharma and J. S. Kim, *Angew. Chemie Int. Ed.*, 2021, **60**, 3196–3204.
50 C. Xu, R. Ye, H. Shen, J. W. Y. Lam, Z. Zhao and B. Zhong Tang, *Angew. Chemie Int. Ed.*, 2022, **61**, e202204604.
51 G. Feng, G.-Q. Zhang and D. Ding, *Chem. Soc. Rev.*, 2020, **49**, 8179–8234.
52 Y. Li, Z. Wang, Y. Qi, Z. Tang, X. Li and Y. Huang, *Chem. Commun.*, 2022, **58**, 8404–8407.
53 F. Amin and B. Bano, *Int. J. Biol. Macromol.*, 2018, **119**, 369–379.
54 R. O. Ogbodu and T. Nyokong, *Spectrochim. Acta Part A Mol. Biomol. Spectrosc.*, 2015, **151**, 174–183.
55 G. Liu, Y. Zhang, H. Yao, Z. Deng, S. Chen, Y. Wang, W. Peng, G. Sun, M. K. Tse, X. Chen, J. Yue, Y. K. Peng, L. Wang and G. Zhu, *Sci. Adv.*, 2023, **9**, eadg5964.
56 N. Wang, Z. Deng, Q. Zhu, J. Zhao, K. Xie, P. Shi, Z. Wang, X. Chen, F. Wang, J. Shi and G. Zhu, *Chem. Sci.*, 2021, **12**, 14353–14362.
57 L. F. Tietze and T. Eicher, *Reaktionen und Synthesen im organisch-chemischen Praktikum und Forschungslaboratorium*, Wiley, 1991.
58 F. Neese, *WIREs Comput. Mol. Sci.*, , DOI:10.1002/wcms.1606.
59 F. Neese, F. Wennmohs, U. Becker and C. Riplinger, *J. Chem. Phys.*, 2020, **152**, Art. No. L224108.
60 T. Lu and F. Chen, *J. Comput. Chem.*, 2012, **33**, 580–592.
61 F. Weigend and R. Ahlrichs, *Phys. Chem. Chem. Phys.*, 2005, **7**, 3297.
62 D. A. Pantazis, X.-Y. Chen, C. R. Landis and F. Neese, *J. Chem. Theory Comput.*, 2008, **4**, 908–919.
63 A. V. Marenich, C. J. Cramer and D. G. Truhlar, *J. Phys. Chem. B*, 2009, **113**, 6378–6396.
64 Y.-J. Tu, D. Njus and H. B. Schlegel, *Org. Biomol. Chem.*, 2017, **15**, 4417–4431.
65 G. Meng, M.-L. Zheng and M. Wang, *Org. Prep. Proced. Int.*, 2011, **43**, 308–311.
66 Y. He, M. Lin, Z. Li, X. Liang, G. Li and J. C. Antilla, *Org. Lett.*, 2011, **13**, 4490–4493.
67 Y. Zhu, C. Chen, G. Yang, Q. Wu, J. Tian, E. Hao, H. Cao, Y. Gao and W. Zhang, *ACS Appl. Mater. Interfaces*, 2020, **12**, 44523–44533.
68 M. Ravera, E. Gabano, S. Tinello, I. Zanellato and D. Osella, *J. Inorg. Biochem.*, 2017, **167**, 27–35.
69 J. Z. Zhang, P. Bonnitcha, E. Wexselblatt, A. V. Klein, Y. Najajreh, D. Gibson and T. W. Hambley, *Chem. – A Eur. J.*, 2013, **19**, 1672–1676.
70 Q. Li, J. Liu, Y. Xu, H. Liu, J. Zhang, Y. Wang, Y. Sun, M. Zhao, L. Liao and X. Wang, *ACS Appl. Mater. Interfaces*, 2022, **14**, 28427–28438.
71 J. Liu, R. Xiao, Y.-L. Wong, X.-P. Zhou, M. Zeller, A. D. Hunter, Q. Fang, L. Liao and Z. Xu, *Inorg. Chem.*, 2018, **57**, 4807–4811.
72 C. Zanato, M. Cascio, P. Lazzari, R. Pertwee, A. Testa and M. Zanda, *Synthesis (Stuttg).*, 2015, **47**, 817–826.
73 H. Dai, G. Liu, X. Zhang, H. Yan and C. Lu, *Organometallics*, 2016, **35**, 1488–1496.
74 M. von Delius, E. M. Geertsema and D. A. Leigh, *Nat. Chem.*, 2010, **2**, 96–101.